



OPEN

SUBJECT AREAS:

FUEL CELLS

CARBON NANOTUBES AND
FULLERENES

ELECTROCATALYSIS

NANOPARTICLES

Received
6 June 2014Accepted
21 August 2014Published
5 September 2014

Correspondence and requests for materials should be addressed to T.F. (fujigaya-tcm@mail.cstm.kyushu-u.ac.jp) or N.N. (nakashima-tcm@mail.cstm.kyushu-u.ac.jp)

Enhancement of Platinum Mass Activity on the Surface of Polymer-wrapped Carbon Nanotube-Based Fuel Cell Electrocatalysts

Inas H. Hafez^{1,4}, Mohamed R. Berber^{1,5}, Tsuyohiko Fujigaya^{1,2} & Naotoshi Nakashima^{1,2,3}

¹International Institute for Carbon-Neutral Energy Research (WPI-I2CNER), Kyushu University, 744 Motooka Nishi-ku, Fukuoka 819-0395, Japan, ²Department of Applied Chemistry, Graduate School of Engineering, Kyushu University, 744 Motooka Nishi-ku, Fukuoka 819-0395, Japan, ³JST-CREST, 5 Sanbancho, Chiyoda-ku, Tokyo, 102-0075, Japan, ⁴Department of Natural resources and Agricultural Engineering, Faculty of Agriculture, Damanhour University, Damanhour 22516, Egypt, ⁵Department of Chemistry, Faculty of Science, Tanta University, Tanta 31527, Egypt.

Cost reduction and improved durability are the two major targets for accelerating the commercialization of polymer electrolyte membrane fuel cells (PEFCs). To achieve these goals, the development of a novel method to fabricate platinum (Pt)-based electrocatalysts with a high mass activity, deposited on durable conductive support materials, is necessary. In this study, we describe a facile approach to grow homogeneously dispersed Pt nanoparticles (Pt) with a narrow diameter distribution in a highly controllable fashion on polymer-wrapped carbon nanotubes (CNTs). A PEFC cell employing a composite with the smallest Pt nanoparticle size (2.3 nm diameter) exhibited a ~8 times higher mass activity compared to a cell containing Pt with a 3.7 nm diameter. This is the first example of the diameter control of Pt on polymer-wrapped carbon supporting materials, and the study opens the door for the development of a future-generation of PEFCs using a minimal amount of Pt.

Polymer electrolyte membrane fuel cells (PEFCs) are considered as one of the best power sources to realize green and efficient energy generation for many commercial applications. PEFCs mainly rely on the use of platinum (Pt) metal because it is the most efficient catalyst for an efficient oxygen reduction reaction (ORR), in addition to its high stability under the strong PEFC acidic conditions^{1,2}. However, Pt is a very expensive and rare. Thus, it is considered a major hinderance to the global commercialization of PEFCs^{1,3,4}.

A widely accepted solution to reduce the cost of PEFCs is the use of a minimal amount of Pt in the electrocatalyst, and thus we need to maximize the mass activity of Pt in the electrocatalyst. The major strategy of increasing the mass activity of Pt is to add a second inexpensive metal to Pt to form either a Pt core-shell⁵⁻⁸ or a Pt alloy in order to increase the surface area of the Pt per unit amount⁹⁻¹⁴. However, it has been pointed out that under the strong acidic environment of the PEFCs, a dissolution process of the second metal occurs resulting in a low fuel cell durability¹⁵⁻²⁰. Another promising strategy towards the increase of Pt mass activity is to reduce the particle size of Pt in order to increase the surface area of the Pt nanoparticles, which can lead to an increase in the mass activity of Pt²¹⁻²³. The simplest technique in decreasing the size of Pt nanoparticles is to minimize the amount of Pt-ions fed into the Pt reduction process in order to regulate the growth of the nanoparticles. Successful examples of the Pt size reduction were reported for carbon black (CB)²³ and graphene oxide²². In both systems, since polar functional groups such as carboxylic and/or hydroxyl groups served as effective binding sites for the Pt ions, the nucleation step occurs homogeneously and, thus, the final Pt size was regulated by simply controlling the feed of Pt ions into the solutions.

However, the oxidized sites of the carbon support accelerate the degradation of the support material, inducing significant aggregation of Pt nanoparticles²⁴. Therefore, novel binding sites with an effective binding of Pt ions on the carbon supports are required for the practical and the commercial use of PEFCs. Recently, we have reported a unique approach for the growth of Pt nanoparticles on non-oxidized graphitic carbon, in which polybenzimidazoles (PBIs) are strongly attached to the surface of CNTs in nanometer thickness, providing effective growth sites for Pt ions²⁵⁻³⁰. Due to the effective binding of Pt ions on PBIs *via* a coordination mechanism, the homo-

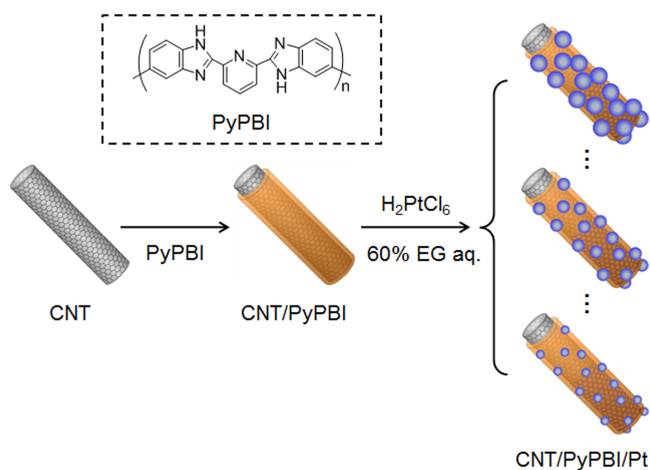


Figure 1 | Schematic drawing describing the preparation of the CNT/PyPBI/Pt composites. A series of CNT/PyPBI/Pt composite were prepared by changing the feeding amount of Pt salt. Chemical structure of PyPBI is presented in the dotted frame.

geneous growth of Pt nanoparticles was realized, and thereby a homogeneous dispersion of Pt catalyst on the supporting material together with a narrow diameter distribution were achieved²⁷. In the present study, we utilized the advantages of our effective binding technique of the Pt ion for the deposition of size-controlled Pt nanoparticles onto the non-oxidized CNT in order to increase the mass activity of Pt in PEFCs.

Poly[2,2'-(2,6-pyridine)-5,5'-bibenzimidazole] (PyPBI; Fig. 1) was used to wrap the CNTs (denoted CNT/PyPBI) because of the following three main reasons: i) this polymer efficiently solubilized the CNTs through $\pi-\pi$ interactions, ii) it is a proton conductor material that can improve the proton conductivity of the electrocatalyst, and iii) it has N-atoms that work as the binding sites for the growth of Pt ions by coordination between the PyPBI and Pt ion²⁵. The Pt was loaded on CNT/PyPBI to prepare Pt composite (denoted CNT/PyPBI/Pt) as displayed in a schematic illustration (Fig. 1)²⁵. For the highest loading of Pt metal, Pt ions corresponding to 50 wt% of the final composite weight was added (denoted CNT/PyPBI/Pt₅₀). The transmission electron microscopic (TEM) image of CNT/PyPBI/Pt₅₀ exhibits a homogeneous loading of Pt metal with diameters of 3.7 ± 0.6 nm (Fig. 2a). The decrease of the feeding amount of the Pt ions to 1/2, 1/5, 1/10 and 1/20 (the obtained composites were denoted CNT/PyPBI/Pt₂₅, CNT/PyPBI/Pt₁₀, CNT/PyPBI/Pt₅ and CNT/PyPBI/Pt_{2.5}, respectively) led to a gradual decrease in the Pt size to 3.6 ± 0.6 , 3.3 ± 0.6 , 2.7 ± 0.6 and 2.3 ± 0.5 nm for CNT/PyPBI/Pt₂₅, CNT/PyPBI/Pt₁₀, CNT/PyPBI/Pt₅ and CNT/PyPBI/Pt_{2.5}, respectively (Figs. 2b~2e). Importantly, the dispersions of the Pt metal on the CNTs were highly homogeneous, as observed from the TEM images (Fig. 2; left images), and the Pt size distributions for all the composites were very narrow (Fig. 2; right). Such an excellent controllability of Pt deposition is probably derived from the rapid nucleation of Pt seed on the PyPBI-wrapped CNTs through the coordination of the Pt ions with the benzimidazole unit of the PyPBI²⁵.

Fig. 3 shows representative scanning electron microscope (SEM) and scanning transmission electron microscope (STEM) images of the CNT/PyPBI/Pt₅₀ (Figs. 3a~3c), CNT/PyPBI/Pt₁₀ (Figs. 3d~3f), and CNT/PyPBI/Pt_{2.5} (Figs. 3g~3i). Comparison of SEM and STEM image allowed us to distinguish the Pt nanoparticles in the front side and in the backside and clarified the decreasing of loading density as decreasing of the Pt feeding. As emphasized by the color contrast in Figs. 3b, 3e, and 3h, we successfully visualized the coating of the PyPBI layers on the CNTs (the green color) as well as small uncoated

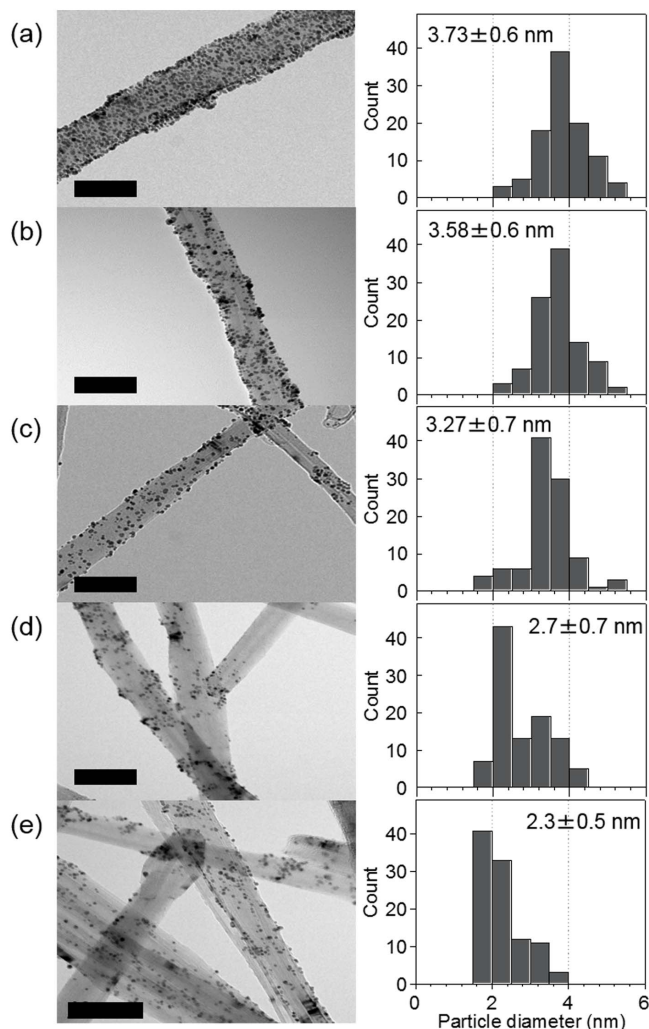


Figure 2 | Pt diameter and distribution analyses of the CNT/PyPBI/Pt. The TEM images (left) and diameter histograms (right) of (a), CNT/PyPBI/Pt₅₀, (b), CNT/PyPBI/Pt₂₅, (c), CNT/PyPBI/Pt₁₀, (d), CNT/PyPBI/Pt₅ and (e), CNT/PyPBI/Pt_{2.5} revealed the diameter of Pt and density of Pt loading were decreased by decreasing the feeding amount of Pt salt with maintaining the homogeneous dispersion of Pt on the CNT/PyPBI. Scale bars, 50 nm.

bare surface spots based on the difference in the scattering efficiency of the PyPBI area and the bare CNT surfaces for the secondary electrons. To the best of our knowledge, this is the first example of visualizing a polymer wrapped on the CNTs by SEM measurements. Importantly, the Pt nanoparticles were observed only on the PyPBI regions, which provided clear evidence that the loading was occurred on the PyPBI layer.

The loading efficiency of Pt was estimated based on the final residues in the thermal gravimetric analysis (TGA) shown in (Fig. 4a), where the loaded Pt was found to be 50, 26, 9, 6 and 4 wt% for CNT/PyPBI/Pt₅₀, CNT/PyPBI/Pt₂₅, CNT/PyPBI/Pt₁₀, CNT/PyPBI/Pt₅ and CNT/PyPBI/Pt_{2.5} composites, respectively. These values correspond to $\sim 100\%$ of the fed Pt ions. From all above results, we concluded that the effective binding of Pt ion onto PyPBI leads the quantitative and homogeneous loading of Pt onto the CNT/PyPBI, thereby the excellent controllability was realized.

The X-ray photoelectron spectroscopy was used to confirm the composite structure of the electrocatalyst and to collect information about the bonding between N-atoms and Pt ions. As observed from the XPS measurements, the N 1s peak at 400 eV³¹ due to PyPBI together with the Pt 4f doublet peaks at 71.1 and 74.4 eV attributable

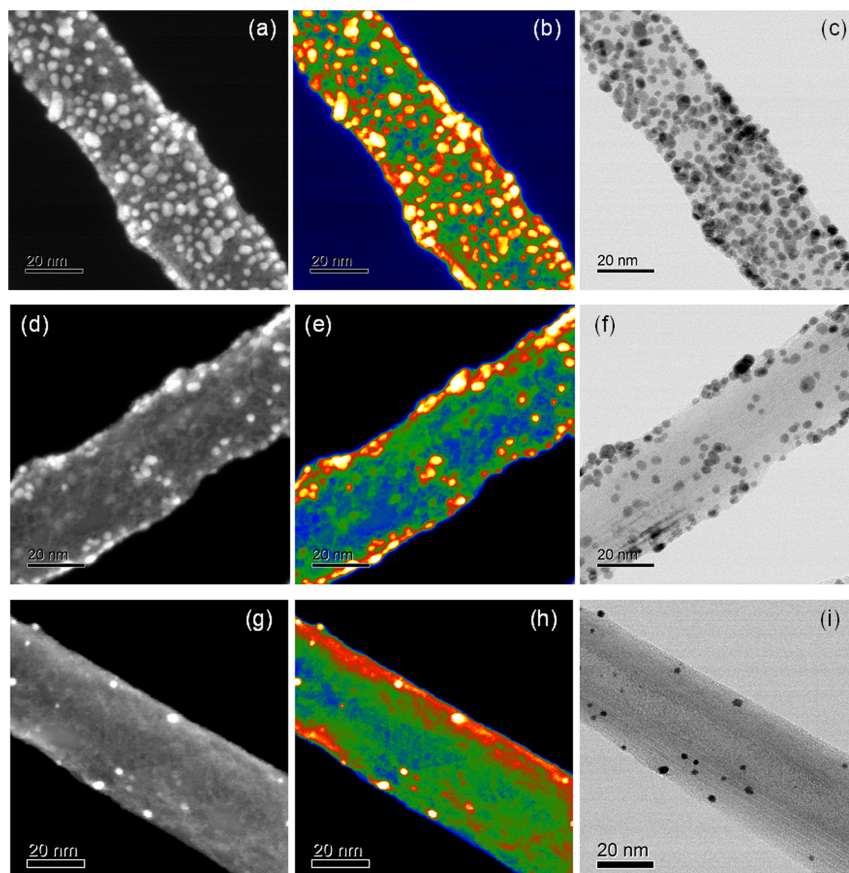


Figure 3 | Electron microscope observations of the CNT/PyPBI/Pt. SEM (a, b, d, e, g, h) and STEM (c, f, i) images of CNT/PyPBI/Pt₅₀ (a~c), CNT/PyPBI/Pt₁₀ (d~f) and CNT/PyPBI/Pt_{2.5} (g~i).

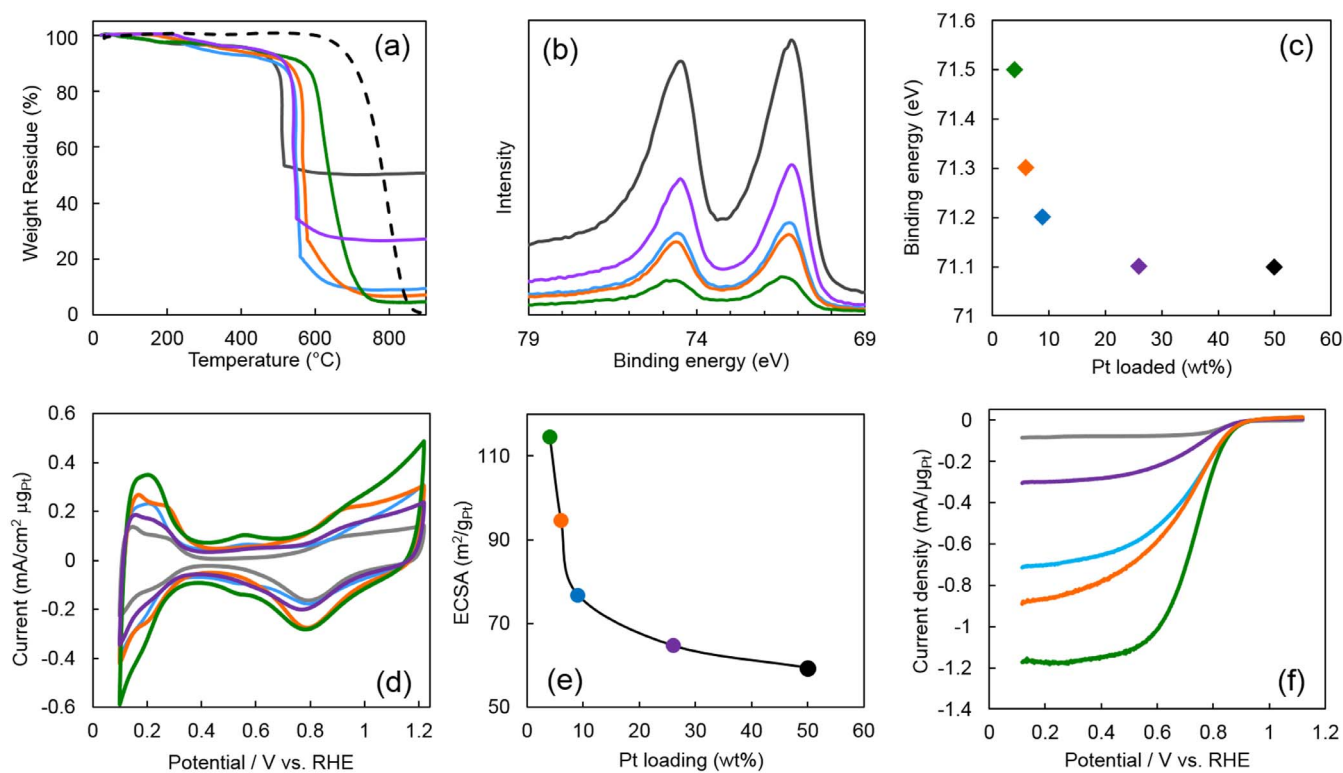
to Pt 4f_{7/2} and Pt 4f_{5/2}, respectively³², are observed in all the prepared composites (Supplementary, Fig. S1). The nitrogen/carbon ratio determined from XPS was recorded to be ~5%, indicating a thin layer of PyPBI on the surface of the CNTs. Together with the decrease in the intensity of the Pt 4f peaks due to the lowering of the Pt loading amount in the composites (Fig. 4b), we recognized an upshift in the Pt 4f peaks with the decrease in Pt size as plotted in Fig. 4c. A similar shift of the Pt 4f peak towards a higher binding energy was also reported for small Pt clusters and this upshift has been attributed to the increase in the number of Pt atoms with low coordination numbers^{22,33,34}.

The electrochemically active surface areas (ECSAs) of Pt nanoparticles in the composites were evaluated by cyclic voltammetry (CV) measurements of loading the same amount of Pt on GC. However, the catalyst layer with the same mass of Pt was unstable on GC during the ORR measurements because the rotation of the GC electrode strongly affected the diffusion process due to the differences of the film thicknesses of the catalysts. Therefore, it was important to measure the ORR of the catalysts with the same film thickness (the same amount of composites). As shown in Fig. 4d, all the composites exhibited clear peaks due to hydrogen adsorption and desorption at 0–0.3 V (vs. RHE). The ECSAs were determined using the hydrogen desorption peak. The determined ECSA values were plotted as a function of the amount of Pt loaded onto the CNT/PyPBI composites (Fig. 4e). As observed, the decrease in the Pt diameter led to a dramatic increase in the ECSA. The highest ECSA value was recorded to be 114.5 m²/g_{Pt} for the CNT/PyPBI/Pt_{2.5} composite, which is comparable to that of Pt of a similar size on graphene oxide²² and CB³⁵, meaning the PyPBI layer has served as a growth site for Pt similar to other oxidized carbon materials. In order to evaluate the Pt utilization efficiency of the prepared electrocatalysts, the ratio of the ECSA

to the calculated theoretical surface area (TSA) of Pt was evaluated. The obtained Pt utilization efficiency values are summarized in Fig. 4g. Interestingly, the reduction of the Pt size has led to an increase in the Pt utilization efficiency. The value reached as high as 94% for the smallest Pt particles in the CNT/PyPBI/Pt_{2.5} electrocatalyst. In addition, the increase in the utilization efficiency revealed a decrease in the contact area of Pt with the PyPBI layers, and also has indicated an increase in the exposed surface of Pt as the Pt diameters decreased.

Watanabe et al. pointed out that, when the Pt nanoparticles are too close to each other (roughly below 1.8 nm for oxygen gas and 2.0 nm for air), a poor diffusion of oxygen is obtained since not all the Pt surface areas are expected to be available for the oxygen reduction reaction (ORR). Consequently, not only the size of Pt, but also the Pt inter-particle distance plays an important role for the increase of the Pt mass activity²³. In our composites, the distributions of the Pt inter-particle distances measured from the TEM images have shifted to higher values (>18 nm) when the loading amounts of Pt were decreased (Supplementary, Fig. S2). Indeed, it was obvious from the ORR (Fig. 4f) that the current density per unit weight of Pt increases with the decrease in the diameter of the Pt nanoparticles.

Furthermore, we have examined the effect of the Pt inter-particle distance and the diameter of the Pt nanoparticles on the Pt-dispersion durability of the composites. The CNT/PyPBI/Pt₅₀ and CNT/PyPBI/Pt_{2.5} composites were measured by an *in situ* SEM/STEM dual monitoring system which is equipped with a gas injection system while heating at 200°C. In these experiments, the composites were heated under vacuum at 3.3×10^{-5} Pa, then atmospheric air (RH = 42%, temp; 24°C) was introduced until the pressure reached 1.2×10^{-2} Pa (for pressure data, Supplementary, Fig. S3) to accelerate the particle activity³⁶. The Pt nanoparticles were found to be quite stable



(g)

Sample Name	Particle size (nm)	ECSA ^{a)} (m ² /g _{Pt})	TSA ^{b)} (m ² /g _{Pt})	Utilization efficiency (%)
CNT/PyPBI/Pt ₅₀	3.7 ± 0.6	59.4	75.6	82.7
CNT/PyPBI/Pt ₂₅	3.6 ± 0.6	64.7	77.8	83.1
CNT/PyPBI/Pt ₁₀	3.3 ± 0.6	76.8	84.8	90.5
CNT/PyPBI/Pt ₅	2.7 ± 0.6	94.5	103.7	91.1
CNT/PyPBI/Pt _{2.5}	2.3 ± 0.5	114.5	121.8	94

^{a)} ECSA = QH/(210 × g_{Pt}) where QH is the charge exchanged during the desorption of hydrogen atoms on Pt, and g_{Pt} is the amount of Pt on the glassy carbon electrode, obtained by loading the same mass of Pt on GC electrode; ^{b)} TSA = 6/pd where p is the density of the platinum metal (21.4 × 10⁶ gm⁻³) and d is the mean diameter of the Pt particle size determined from the TEM.

Figure 4 | TGA, XPS and electrochemical measurements of the CNT/PyPBI/Pt as well as their numerical data. (a), TGA curves of CNT/PyPBI/Pt₅₀ (gray), CNT/PyPBI/Pt₂₅ (purple), CNT/PyPBI/Pt₁₀ (blue), CNT/PyPBI/Pt₅ (orange) and CNT/PyPBI/Pt_{2.5} (green). TGA curve of CNT (dotted line) is also displayed as a reference. (b), XPS narrow scans of Pt 4f for CNT/PyPBI/Pt₅₀ (gray), CNT/PyPBI/Pt₂₅ (purple), CNT/PyPBI/Pt₁₀ (blue), CNT/PyPBI/Pt₅ (orange) and CNT/PyPBI/Pt_{2.5} (green). (c), The relation between the Pt loaded on the polymer-wrapped CNT composites and the binding energy of Pt 4f. (d), CV of CNT/PyPBI/Pt₅₀ (gray), CNT/PyPBI/Pt₂₅ (purple), CNT/PyPBI/Pt₁₀ (blue), CNT/PyPBI/Pt₅ (orange) and CNT/PyPBI/Pt_{2.5} (green). (e), Plot of ECSA values as a function of the Pt loading. (f), LSV of the CNT/PyPBI/Pt₅₀ (gray), CNT/PyPBI/Pt₂₅ (purple), CNT/PyPBI/Pt₁₀ (blue), CNT/PyPBI/Pt₅ (orange) and CNT/PyPBI/Pt_{2.5} (green). (g), list of particle size, ECSA, TSA and utilization efficiency for the CNT/PyPBI/Pt.

at 200°C under high vacuum conditions for both composites but when the air was introduced, the migration of the Pt on the surfaces of the CNTs gradually started to form bigger particles by Pt fusion on the surface of the CNTs (Supplementary, Movies 1 and 2). Such phenomena are in sharp contrast to that of Pt on CB, in which the Pt is inserted into the CB support, and then a Pt agglomeration process occurs inside the carbon³⁶. This difference in the Pt behaviour on the CNT and CB supports would be due to the higher stability of the CNTs towards the catalytic oxidation of carbon by Pt in air.

In order to compare the difference in the Pt-dispersion stability of the CNT/PyPBI/Pt₅₀ and CNT/PyPBI/Pt_{2.5} composites, snapshots of the two composites were extracted from videos in the pressure ranges

of $4 \times 10^{-5} \sim 9 \times 10^{-4}$ Pa (Fig. 5a) and $1 \times 10^{-3} \sim 5 \times 10^{-3}$ Pa (Fig. 5b). Notably, the Pt in the CNT/PyPBI/Pt₅₀ started to move from around 6×10^{-4} Pa (Fig. 5a), whereas the Pt in the CNT/PyPBI/Pt₅ was stable even below 3×10^{-3} Pa. Furthermore, a number of small Pt nanoparticles still remained in the CNT/PyPBI/Pt₅, probably due to the lower density of the Pt nanoparticles on the CNTs (Fig. 5b), which lowered the chance of aggregation. This finding has provided a practical and useful strategy to suppress Pt aggregation caused by migration during fuel cell operations.

A series of membrane-electrode assemblies (MEAs) using CNT/PyPBI/Pt₅₀, CNT/PyPBI/Pt₁₀ or CNT/PyPBI/Pt_{2.5} for both the anode and cathode (denoted MEA₅₀, MEA₁₀ and MEA_{2.5}, respectively) were fabricated in order to investigate the fuel cell performance



carried out under dry conditions at 120 °C. The same amounts of the composites were loaded on the electrocatalyst layers to prepare the electrode catalyst with similar thickness ($\sim 10 \mu\text{m}$), which means that different amounts of Pt corresponding to 0.50, 0.09 and 0.04 mg/cm^2 of Pt were loaded for MEA₅₀, MEA₁₀ and MEA_{2.5}, respectively. The small Pt loading values of MEA₁₀ and MEA_{2.5} (0.09 and 0.04 mg/cm^2) were lower than those of current PEFCs, in which the Pt amounts are 0.4–1.0 mg/cm^2 ²³⁷. The I-V curves together with their power density curves for the MEA₅₀ (gray), MEA₁₀ (blue) and MEA_{2.5} (green) are shown in Fig. 6a. The I-V curves were re-plotted based on the total amounts of Pt in the anode and cathode to compare the Pt mass activity of the MEAs (Fig. 6b). Importantly, the mass activity of MEA_{2.5}, was around 8 times greater than that of MEA₅₀. Fine control of the Pt size strongly indicates a correlation of Pt nanoparticle size with the feed of Pt ions, and further improvements in the mass activity of the MEA is expected^{38,39}; however, several reports have pointed out that smaller-sized Pt particles (<2 nm) show a lower ORR activity, and these are not suitable for the fuel catalysts^{1,40–42}.

In order to shed some light on the stability of the electrocatalysts, the durability of the MEA₁₀ was compared to that of the MEA₅₀. Figs. 7a and 7b show the potential curves of the MEA₅₀ and MEA₁₀ as a function of cycling, respectively. In order to avoid a complex graph, only representative curves of the cycling were selected for display. The durability test was terminated after 60,000 potential cyclings. The potential at 200 mA mgPt^{-1} for both the MEA₅₀ and MEA₁₀ as a function of cycling is displayed in Fig. 7c. As observed, the degradation rates of both MEAs were almost the same, indicating a good stability of the low Pt loading composites. A more detailed study using half-cell measurements is now undergoing.

In conclusion, this is the first example of fine control of Pt nanoparticle diameter on polymer-wrapped carbon supporting materials.

The results showed that the ECSA values were dramatically increased and the utilization efficiency of the Pt was also increased. To compare the mass activity of Pt, we fabricated different MEAs using the prepared electrocatalysts with different Pt diameters. The I-V measurements at 120 °C under the non-humidified condition revealed that the MEA using the smallest Pt (diameter=2.3 nm) showed a mass activity about 8 times higher than that of the MEA using the largest Pt particles (diameter=3.7 nm) due to the significant increase in the surface area of Pt as well as their utilization efficiency. Such a fine control of the ‘Pt size/size reduction and density’ in a simple approach for pristine CNTs is highly useful for the development of a next generation fuel cell electrocatalyst, in which in which the reduction of the Pt amount is highly demanded.

Methods

Materials. *N,N*-Dimethylacetamide (DMAc), ethylene glycol (EG), and hydrogen hexachloroplatinate hexahydrate ($\text{H}_2\text{PtCl}_6 \cdot 6\text{H}_2\text{O}$) were purchased from Wako Pure Chemical, Ltd., and used as received. Multi-walled carbon nanotubes (ca. 20 nm diameter) were kindly donated by the Nikkiso Co. Poly[2,2'-(2,6-pyridine)-5,5'-bibenzimidazole] (PyPBI) and poly[2,2'-(2,6-phenyl)-5,5'-bibenzimidazole] (PBI) were synthesized according to the literature⁴³. CNTs wrapped with PyPBI (denoted CNT/PyPBI) were prepared according to the method described in our previous report²⁵.

Measurements. The size and distribution of the Pt nanoparticles were determined using TEM images (JEOL JEM-2010, acceleration voltage = 120 kV). A copper grid with a carbon support (Okenshoji) was used for the TEM observations. Samples were dispersed in 2-propanol in an ultrasonic bath for 10 min, and a drop of the suspension was placed on a copper grid coated with a carbon film. The copper grid was then dried in a vacuum overnight. The TGA diagrams were obtained using a TGA-50 (Shimadzu) instrument operated in conditioned air (20 mL min^{-1}) at a heating rate of 10 °C min^{-1} . The XRD and XPS spectra were measured using a SmartLab (Rigaku) and AXIS-ULTRA^{DL} (SIMADZU), respectively. The binding energy in the XPS spectra was calibrated using the C 1s peak that appeared at 284.5 eV. Simultaneous SEM and STEM (SEM/STEM dual monitoring system operated at an

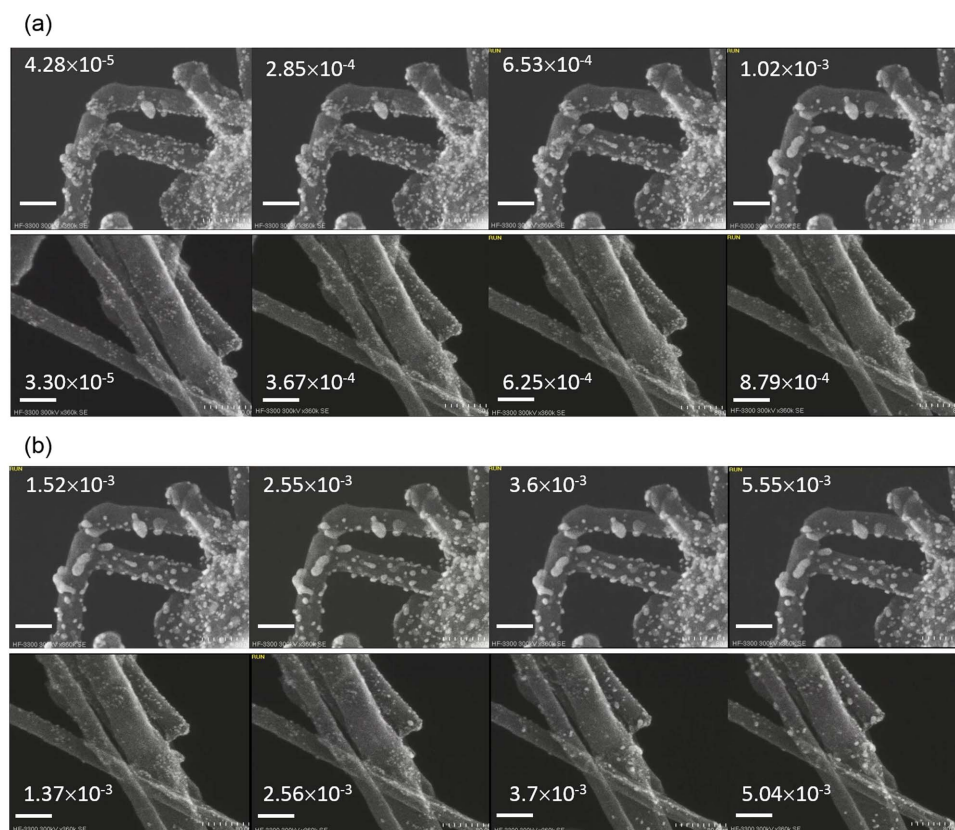


Figure 5 | In situ stability test of Pt dispersion under the electron microscope measurements. (a), (b), Snapshots extracted from the videos (Supplementary, Movies S1 and 2) of the CNT/PyPBI/Pt₅₀ (upper a and b) and CNT/PyPBI/Pt₅ (lower a and b) in the pressure ranges of (a), from 4.28×10^{-5} to 8.79×10^{-4} Pa and (b), from 1.52×10^{-3} to 5.04×10^{-3} Pa. Scale bars, 50 nm.

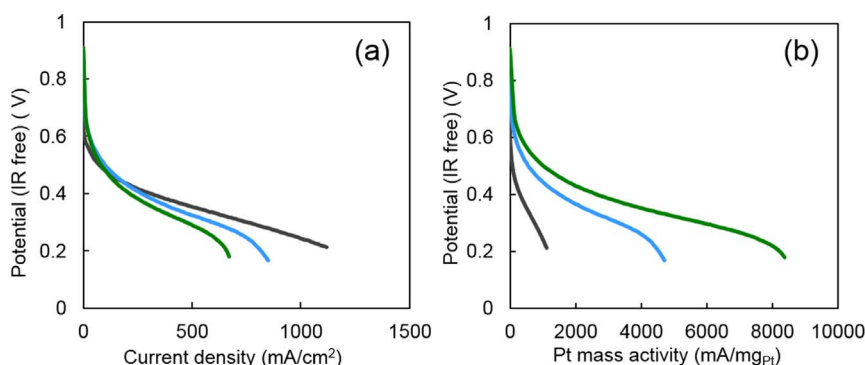


Figure 6 | MEA single cell measurements using CNT/PyPBI/Pt as the electrocatalyst. (a), I-V curves and power density curves for MEA₅₀ (gray), MEA₁₀ (blue) and MEA_{2.5} (green) plotted as a function of the current density. (b), I-V curves for MEA₅₀ (gray), MEA₁₀ (blue) and MEA_{2.5} (green) plotted as a function of Pt mass activity.

acceleration voltage of 300 kV) observations were carried out using an HF-3300 (Hitachi High Technologies) microscope equipped with a gas injection system. In these experiments, the composites were heated up 200 °C under vacuum at 3.3×10^{-5} Pa, then atmospheric air (RH = 42%, temp; 24 °C) was introduced until the pressure reached 1.2×10^{-2} Pa (for pressure data, Supplementary, Fig. S3)

Synthesis of CNT/PyPBI/Pt electrocatalysts. Pt was deposited on the CNT/PyPBI using EG as a reducing agent⁴⁴. Typically, CNT/PyPBI (10 mg) in a 60 vol% aqueous EG solution (60 mL) was dispersed by sonication to which $\text{H}_2\text{PtCl}_6 \cdot 6\text{H}_2\text{O}$ in a 60 vol% aqueous EG solution (1.15 mM; 40 mL) was added. The resultant mixture was stirred for 4 h at room temperature, then refluxed at 140 °C for 8 h. The obtained material was filtered using a 0.2 μm Millipore membrane, washed several times with water, and finally dried under vacuum. The amount (volume) of the aqueous $\text{H}_2\text{PtCl}_6 \cdot 6\text{H}_2\text{O}$ solution added to the solution was changed in order to optimize the amounts of the Pt loaded on the CNT/PyPBI.

Preparation of phosphoric acid doped-PBI membrane. LiBr (100 mg) was dissolved in DMAc (10 mL) in a 50 mL glass bottle to which PBI (200 mg) was added. The bottle was sealed under N_2 and magnetically stirred at 50 °C for 1 day, then

the solvent was evaporated to obtain a solution (PBI content = ~4 wt%). The resultant PBI polymer solution was carefully cast on a glass plate using a film applicator (Elcometer 3600, 50 μm strip width), then gradually heated to 120 °C to evaporate DMAc and held at 120 °C for another 5 h to completely remove the solvent. The obtained PBI film was peeled off and immersed in hot distilled water for 30 min several times to remove the LiBr. Finally, the PBI membrane was doped in a 85-wt% phosphoric acid solution for 5 days to provide a membrane film with a 30- μm thickness. The amount of H_3PO_4 loaded on the membrane after doping was calculated by the weight change from the original membrane.

Electrochemical measurements. Electrochemical measurements were performed using a rotating ring disk electrode (RRDE-3, Bioanalytical Systems, Inc.) with a conventional three-electrode configuration at room temperature. A glassy carbon electrode (GC) with a geometric surface area of 0.282 cm^2 was used as the working electrode. A Pt wire and Ag/AgCl were used as the counter and reference electrodes, respectively. The Ag/AgCl reference electrode was calibrated against the reference hydrogen electrode (RHE) potential in 0.1 M HClO_4 . All work potentials are indicated against the RHE. The potential of the sample electrode was controlled by a potentiostat (Model DY2323, ALS). The catalyst suspension was prepared as follows.

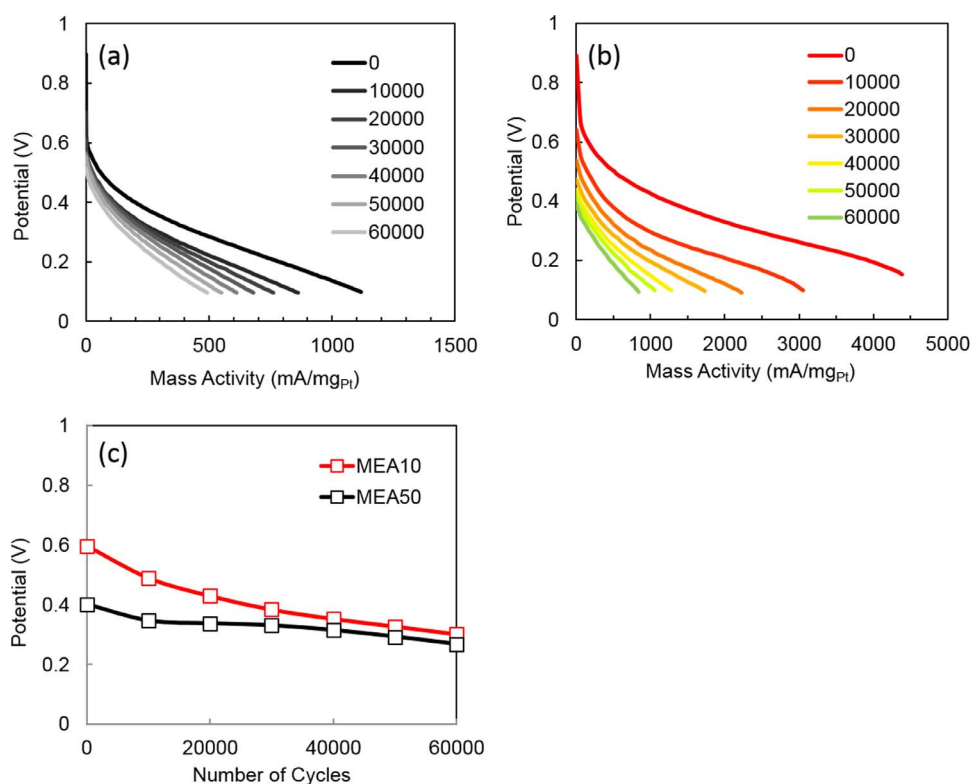


Figure 7 | Durability test of MEA. (a), (b), Polarization curves of a durability test using MEA₅₀ (a) and MEA₁₀ (b). The polarization curves were measured after every 1,000 cycles. For convenience, the data were plotted every 10,000 cycles. (c), Plots of the cell voltage at 200 mA mgPt^{-1} for the MEA₅₀ and MEA₁₀.



CNT/PyPBI/Pt (1.0 mg) was ultrasonically dispersed in an aqueous EG solution (2.0 mL) to provide a homogeneous suspension. A portion of the composite suspension was then cast onto the GC electrode to load $14 \mu\text{g cm}^{-2}$ of Pt for CV measurements, and $40 \mu\text{L}$ of the suspension was cast on a GC electrode for the ORR measurements. Finally, the casted GC electrodes were air dried. The CVs of the electrocatalysts were carried out at a scan rate of 50 mV/sec in N_2 -saturated 0.1 M HClO_4 solutions to determine the ECSA values.

Fuel cell testing. The electrocatalyst composite was ultrasonically dispersed in an aqueous EG solution, then deposited on a gas diffusion layer (GDL) (SIGRACET gas diffusion media GDL 25 BC, SGL Carbon Group) by vacuum filtration. The GDL was used as a filter to produce a gas diffusion electrode (GDE). The H_3PO_4 doped-PBI membrane was then sandwiched between two GDEs to fabricate a membrane-electrode-assembly (MEA). The obtained MEA was hot-pressed at 120°C and 5 MPa for 30 sec. The performance of the MEA was measured at 120°C using a computer-controlled fuel cell test system (890e, Scribner Associate, Inc.). Polarization curves were recorded at atmospheric pressure under a dry hydrogen flow (100 mL/min) and air flow (200 mL/min) as the anode and cathode gases, respectively.

Durability testing. Selected MEAs were subject to an accelerated durability test by the protocol provided by the Fuel Cell Commercialization of Japan (FCCJ)⁴⁵. Typically, the potential sweeps were cycled between 1.0 and 1.5 V at 120°C under non-humidified conditions in order to accelerate the oxidation process. The scanning rate was 0.5 V/s . The H_2 and N_2 gases were fed to the anode and the cathode, respectively. The I-V curves were recorded every 1,000 cycles after switching the cathode gas from N_2 to air. The potential was plotted as a function of cycling at open circuit potential (OCV). The durability test for the examined MEAs was terminated when the potential became less than 50% of the initial OCV.

- Debe, M. K. Electrocatalyst approaches and challenges for automotive fuel cells. *Nature* **486**, 43–51 (2012).
- Tiwari, J. N. *et al.* Stable platinum nanoclusters on genomic DNA–graphene oxide with a high oxygen reduction reaction activity. *Nat Commun* **4** (2013).
- Sun, X. *et al.* A Class of High Performance Metal-Free Oxygen Reduction Electrocatalysts based on Cheap Carbon Blacks. *Sci. Rep.* **3** (2013).
- Jaouen, F. *et al.* Recent advances in non-precious metal catalysis for oxygen-reduction reaction in polymer electrolyte fuel cells. *Energy Environ. Sci.* **4**, 114–130 (2011).
- Beard, K. D. *et al.* Preparation and Structural Analysis of Carbon-Supported Co Core/Pt Shell Electrocatalysts Using Electroless Deposition Methods. *ACS Nano* **3**, 2841–2853 (2009).
- Sasaki, K. *et al.* Core-Protected Platinum Monolayer Shell High-Stability Electrocatalysts for Fuel-Cell Cathodes. *Angew. Chem. Int. Ed.* **49**, 8602–8607 (2010).
- Wang, J. X. *et al.* Oxygen Reduction on Well-Defined Core–Shell Nanocatalysts: Particle Size, Facet, and Pt Shell Thickness Effects. *J. Am. Chem. Soc.* **131**, 17298–17302 (2009).
- Wang, D. *et al.* Facile Synthesis of Carbon-Supported Pd–Co Core–Shell Nanoparticles as Oxygen Reduction Electrocatalysts and Their Enhanced Activity and Stability with Monolayer Pt Decoration. *Chem. Mater.* **24**, 2274–2281 (2012).
- Lim, B. *et al.* Pd–Pt Bimetallic Nanodendrites with High Activity for Oxygen Reduction. *Science* **324**, 1302–1305 (2009).
- Wu, J. *et al.* Truncated Octahedral Pt₃Ni Oxygen Reduction Reaction Electrocatalysts. *J. Am. Chem. Soc.* **132**, 4984–4985 (2010).
- Wang, C., Daimon, H. & Sun, S. Dumbbell-like Pt–Fe₃O₄ Nanoparticles and Their Enhanced Catalysis for Oxygen Reduction Reaction. *Nano Lett.* **9**, 1493–1496 (2009).
- Li, Y., Qi, W., Huang, B., Ji, W. & Wang, M. Size- and Composition-Dependent Structural Stability of Core–Shell and Alloy Pd–Pt and Au–Ag Nanoparticles. *J. Phys. Chem. C* **117**, 15394–15401 (2013).
- Gasteiger, H. A., Kocha, S. S., Sompalli, B. & Wagner, F. T. Activity benchmarks and requirements for Pt, Pt-alloy, and non-Pt oxygen reduction catalysts for PEMFCs. *Appl. Catal. B* **56**, 9–35 (2005).
- Zhang, J. *et al.* Platinum Monolayer Electrocatalysts for O₂ Reduction: Pt Monolayer on Pd(111) and on Carbon-Supported Pd Nanoparticles. *J. Phys. Chem. B* **108**, 10955–10964 (2004).
- Oezaslan, M., Hasché, F. & Strasser, P. Pt-Based Core–Shell Catalyst Architectures for Oxygen Fuel Cell Electrodes. *J. Phys. Chem. Lett.* **4**, 3273–3291 (2013).
- Colon-Mercado, H. R. & Popov, B. N. Stability of platinum based alloy cathode catalysts in PEM fuel cells. *J. Power Sources* **155**, 253–263 (2006).
- Stamenkovic, V. R., Mun, B. S., Mayrhofer, K. J. J., Ross, P. N. & Markovic, N. M. Effect of Surface Composition on Electronic Structure, Stability, and Electrocatalytic Properties of Pt–Transition Metal Alloys: Pt–Skin versus Pt–Skeleton Surfaces. *J. Am. Chem. Soc.* **128**, 8813–8819 (2006).
- Stamenkovic, V. R. *et al.* Improved Oxygen Reduction Activity on Pt₃Ni(111) via Increased Surface Site Availability. *Science* **315**, 493–497 (2007).
- Stephens, I. E. L., Bondarenko, A. S., Gronbjerg, U., Rossmeisl, J. & Chorkendorff, I. Understanding the electrocatalysis of oxygen reduction on platinum and its alloys. *Energy Environ. Sci.* **5**, 6744–6762 (2012).

- Hwang, S. J. *et al.* Role of Electronic Perturbation in Stability and Activity of Pt-Based Alloy Nanocatalysts for Oxygen Reduction. *J. Am. Chem. Soc.* **134**, 19508–19511 (2012).
- Fang, B., Chaudhari, N. K., Kim, M.-S., Kim, J. H. & Yu, J.-S. Homogeneous Deposition of Platinum Nanoparticles on Carbon Black for Proton Exchange Membrane Fuel Cell. *J. Am. Chem. Soc.* **131**, 15330–15338 (2009).
- Sibirian, R., Kondo, T. & Nakamura, J. Size Control to a Sub-Nanometer Scale in Platinum Catalysts on Graphene. *J. Phys. Chem. C* **117**, 3635–3645 (2013).
- Watanabe, M., Sei, H. & Stonehart, P. The influence of platinum crystallite size on the electroreduction of oxygen. *J. Electroanal. Chem. Interfacial Electrochem.* **261**, 375–387 (1989).
- Wang, X., Li, W., Chen, Z., Waje, M. & Yan, Y. Durability investigation of carbon nanotube as catalyst support for proton exchange membrane fuel cell. *J. Power Sources* **158**, 154–159 (2006).
- Fujigaya, T., Okamoto, M. & Nakashima, N. Design of an assembly of pyridine-containing polybenzimidazole, carbon nanotubes and Pt nanoparticles for a fuel cell electrocatalyst with a high electrochemically active surface area. *Carbon* **47**, 3227–3232 (2009).
- Fujigaya, T., Okamoto, M., Matsumoto, K., Kaneko, K. & Nakashima, N. Interfacial engineering of platinum catalysts for fuel cells: Methanol oxidation is dramatically improved by polymer coating on a platinum catalyst. *ChemCatChem* **5**, 1701–1704 (2013).
- Fujigaya, T. & Nakashima, N. Fuel Cell Electrocatalyst Using Polybenzimidazole-Modified Carbon Nanotubes As Support Materials. *Adv. Mater.* **25**, 1666–1681 (2013).
- Fujigaya, T., Kim, C., Matsumoto, K. & Nakashima, N. Effective anchoring of Pt-nanoparticles onto sulfonated polyelectrolyte-wrapped carbon nanotubes for use as a fuel cell electrocatalyst. *Polym J* **45**, 326–330 (2013).
- Berber, M. R., Fujigaya, T., Sasaki, K. & Nakashima, N. Remarkably Durable High Temperature Polymer Electrolyte Fuel Cell Based on Poly(vinylphosphonic acid)-doped Polybenzimidazole. *Sci. Rep.* **3** (2013).
- Matsumoto, K., Fujigaya, T., Sasaki, K. & Nakashima, N. Bottom-up design of carbon nanotube-based electrocatalysts and their application in high temperature operating polymer electrolyte fuel cells. *J. Mater. Chem.* **21**, 1187–1190 (2011).
- Hamilton, L. E., Sherwood, P. M. A. & Reagan, B. M. X-ray photoelectron spectroscopy studies of photochemical changes in high-performance fibers. *Appl. Spectrosc.* **47**, 139–149 (1993).
- Tian, Z. Q., Jiang, S. P., Liang, Y. M. & Shen, P. K. Synthesis and Characterization of Platinum Catalysts on Multiwalled Carbon Nanotubes by Intermittent Microwave Irradiation for Fuel Cell Applications. *J. Phys. Chem. B* **110**, 5343–5350 (2006).
- Toyoda, E. *et al.* The d-Band Structure of Pt Nanoclusters Correlated with the Catalytic Activity for an Oxygen Reduction Reaction. *J. Phys. Chem. C* **115**, 21236–21240 (2011).
- Kondo, T., Suzuki, T. & Nakamura, J. Nitrogen Doping of Graphite for Enhancement of Durability of Supported Platinum Clusters. *J. Phys. Chem. Lett.* **2**, 577–580 (2011).
- Zhang, S. & Chen, S. Enhanced-electrocatalytic activity of Pt nanoparticles supported on nitrogen-doped carbon for the oxygen reduction reaction. *J. Power Sources* **240**, 60–65 (2013).
- Matsumoto, H. *et al.* Simultaneous in situ SEM and STEM analysis of gas/catalyst reaction in a cold field-emission environmental TEM. *Microscopy and Analysis*, 13–18 (2013).
- Cho, Y.-H. *et al.* Effect of platinum amount in carbon supported platinum catalyst on performance of polymer electrolyte membrane fuel cell. *J. Power Sources* **172**, 89–93 (2007).
- Imaoka, T. *et al.* Magic Number Pt₁₃ and Misshapen Pt₁₂ Clusters: Which One is the Better Catalyst? *J. Am. Chem. Soc.* **135**, 13089–13095 (2013).
- Yamamoto, K. & Imaoka, T. Precision Synthesis of Subnanoparticles Using Dendrimers as a Supramolecular Synthesizer. *Acc. Chem. Res.* (2014).
- Kinoshita, K. Particle Size Effects for Oxygen Reduction on Highly Dispersed Platinum in Acid Electrolytes. *J. Electrochem. Soc.* **137**, 845–848 (1990).
- Nesselberger, M. *et al.* The Particle Size Effect on the Oxygen Reduction Reaction Activity of Pt Catalysts: Influence of Electrolyte and Relation to Single Crystal Models. *J. Am. Chem. Soc.* **133**, 17428–17433 (2011).
- Mayrhofer, K. J. J. *et al.* The Impact of Geometric and Surface Electronic Properties of Pt-Catalysts on the Particle Size Effect in Electrocatalysis. *J. Phys. Chem. B* **109**, 14433–14440 (2005).
- Carollo, A. *et al.* Developments of new proton conducting membranes based on different polybenzimidazole structures for fuel cells applications. *J. Power Sources* **160**, 175–180 (2006).
- Li, W. *et al.* Preparation and Characterization of Multiwalled Carbon Nanotube-Supported Platinum for Cathode Catalysts of Direct Methanol Fuel Cells. *J. Phys. Chem. B* **107**, 6292–6299 (2003).
- Ohma, A. *et al.* Membrane and Catalyst Performance Targets for Automotive Fuel Cells by FCCJ Membrane, Catalyst, MEA WG. *ECS Transactions* **41**, 775–784 (2011).

Acknowledgments

The authors gratefully acknowledge Prof. A. Robertson of Kyushu University for helpful discussion and H. Matsumoto and T. Sato of Hitachi High-Technologies Corporation for



the measurements of SEM/STEM dual monitoring. This work was supported in part by the Low-Carbon Research Network (LCnet) and the Nanotechnology Platform Project of the Ministry of Education, Japan. Part of this research was supported by the Adaptable and Seamless Technology Transfer Program through Target-driven R&D, JST (AS242Z00200L) and the Advanced Low Carbon Technology Research and Development Program (ALCA).

Author contributions

T.F. and N.N. proposed and supervised the project. I.H.H. and M.R.B. carried out experiments. I.H.H., M.R.B., T.F. and N.N. wrote the manuscript.

Additional information

Supplementary information accompanies this paper at <http://www.nature.com/scientificreports>

Competing financial interests: The authors declare no competing financial interests.

How to cite this article: Hafez, I.H., Berber, M.R., Fujigaya, T. & Nakashima, N. Enhancement of Platinum Mass Activity on the Surface of Polymer-wrapped Carbon Nanotube-Based Fuel Cell Electrocatalysts. *Sci. Rep.* 4, 6295; DOI:10.1038/srep06295 (2014).



This work is licensed under a Creative Commons Attribution-NonCommercial-NoDerivs 4.0 International License. The images or other third party material in this article are included in the article's Creative Commons license, unless indicated otherwise in the credit line; if the material is not included under the Creative Commons license, users will need to obtain permission from the license holder in order to reproduce the material. To view a copy of this license, visit <http://creativecommons.org/licenses/by-nc-nd/4.0/>